Manipulating magnons via ultrafast magnetization modulation

N. Singh,[1] P. Elliott,[1,*] J. K. Dewhurst,[2] and S. Sharma[1]
[1]*Max-Born-Institut für Nichtlineare Optik und Kurzzeitspektroskopie, Max-Born-Strasse 2A, D-12489 Berlin, Germany*
[2]*Max-Planck-Institut für Mikrostrukturphysik, Weinberg 2, D-06120 Halle, Germany*

(Received 3 July 2019; revised 19 October 2020; accepted 27 January 2021; published 1 April 2021)

We demonstrate how fundamental properties of magnons may be manipulated using femtosecond laser pulses by performing *ab initio* real-time time-dependent density functional theory simulations. To illustrate this, we show how the spin-wave dynamics in $Fe_{50}Ni_{50}$ can be manipulated in three different ways by tailoring the applied laser pulse to excite optically induced intersublattice transfer (OISTR): (1) element-selective destruction of magnon modes depending on the laser intensity, (2) delay-dependent freezing of the magnon mode into a transient noncollinear state (where the delay is in the pulse peak with respect to the start of simulations), and (3) OISTR-driven renormalization of the optical magnon frequency. Harnessing such processes would significantly speed up magnonic devices.

DOI: 10.1103/PhysRevB.103.134402

I. INTRODUCTION

Ultrashort laser technology has emerged as an unexpected, but extremely promising, tool for manipulating the magnetic properties of materials on femtosecond (fs) timescales. The laser light excites the material's constituent electrons into a nonequilibrium state, which then alters the magnetic properties. This is due to the fact that, fundamentally, magnetism arises due to the angular momentum of the electrons, especially the intrinsic angular momentum or spin moment of the electrons. Thus, the interaction between light and electrons may be used to influence the spin dynamics and hence magnetic properties of materials. If such processes can be successfully exploited, they may lead to electronic devices operating at speeds several orders of magnitude faster than those currently available.

Similarly, the last few decades have seen the development of the separate field of spintronics, where manipulating the spin of the electron is established as fundamental to realizing the next technological leap forward in terms of speed, size, and energy efficiency. One of the physical phenomena studied in spintronics is the collective, low-energy (approximately meV), spin-wave quasiparticle excitations known as magnons. These spin waves have several favorable properties [1], such as carrying spin currents without suffering from the limitations encountered by charge currents in conventional electronics. However, it is not known how magnons react to ultrafast changes in the magnetization due to applied laser pulses. Thus, the goal of this work is to investigate how magnon modes respond to ultrafast laser pulses, thus extending magnonics into the fs regime.

As the system is strongly excited by the pump laser, a theoretical method valid in the nonlinear regime is required in order to simulate such a situation. However, the usual theoretical approach to study magnons, atomistic spin dynamics using the Heisenberg model [2] combined with the Landau-Lifshitz-Gilbert equation of motion [3–5], is not applicable in this situation. This is due to the dependence on parameterized exchange interactions which assume that the system is in its ground state and the applied perturbation is very small. In such a situation the exchange parameters can be extracted from *ab initio* density functional theory calculations. However, when the system is pumped into a nonequilibrium state, this is no longer the case, and another method must be used. In this work we will use the *ab initio* method of time-dependent density functional theory (TDDFT).

TDDFT is a formally exact method for treating the dynamics of many-electron systems under the influence of external perturbations [6–8]. TDDFT was recently shown to successfully predict many processes in spin dynamics; in particular optical intersublattice spin transfer (OISTR) was predicted in Refs. [9–11] and then demonstrated experimentally across a wide range of materials and geometries, such as bulk Heusler compounds [12], Co/Cu interfaces [13], Ni/Pt multilayers [14], and Co/Pt alloys [15]. For magnon physics, TDDFT was previously used in the linear regime to predict magnon frequencies and lifetimes [16–18]. It was recently extended to treat magnons in real-time by the authors [19], among others [20], which allows the present work to go a step further and observe the effect of nonlinear perturbation on the magnon modes.

While a number of key mechanisms for altering spin dynamics using ultrafast laser pulses have been identified, e.g., ultrafast demagnetization [21], whereby loss of spin (or magnetic moment) occurs in less than 100 fs when acted upon by an optical laser pulse or all-optical switching [22,23] in which the spins switch by 180° when excited by the laser, for this work we will focus on the previously mentioned OISTR process. The defining signature of OISTR is the transfer of

*peter.elliot@mbi-berlin.de

spin from one atom to another, thus modulating the local magnetic moment and disrupting the magnetic interactions between the electrons, both of which may alter the magnon spin-wave states. As these excitations are directly induced by the pump laser, they take place on the timescale of the laser, typically a few femtoseconds. Therefore, the question to be answered is whether this process can be used to manipulate magnon dynamics on fs timescales.

Below we will show three examples of how OISTR can be used to manipulate magnon modes. We demonstrate (1) element-selective destruction of magnon modes in multicomponent magnetic materials, (2) element-selective canting of the magnetic moment, i.e., a laser-induced transient noncollinear state, and (3) a frequency change in selected magnon modes. The system we choose to demonstrate these examples is the frequently studied $Fe_{50}Ni_{50}$ alloy. It is a multisublattice ferromagnet and is known to display OISTR excitations [24] and to have element-specific magnetization dynamics [25,26], making it a good candidate for the present study.

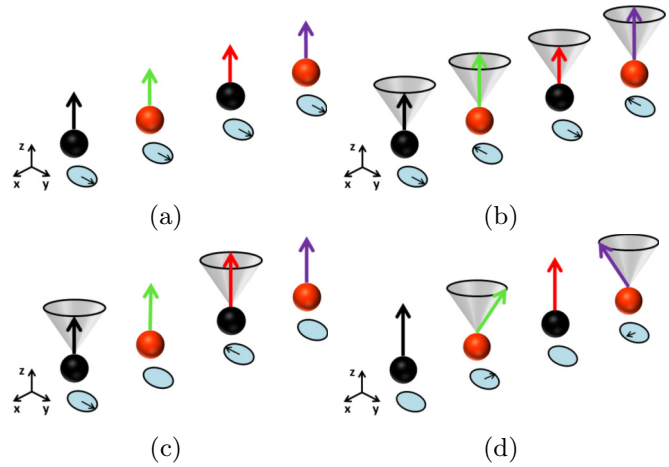

FIG. 1. The four observed modes in a four-atom supercell of the ferromagnetic alloy $Fe_{50}Ni_{50}$. (a) Goldstone mode, (b) optical mode, (c) pure iron mode, and (d) pure nickel mode.

II. THEORETICAL BACKGROUND AND COMPUTATIONAL DETAILS

The fundamental quantities in TDDFT are the density and the magnetization density, which are defined as

$$n(\mathbf{r},t) = \sum_{i=1}^{N} |\phi_i(\mathbf{r},t)|^2,$$

$$\mathbf{m}(\mathbf{r},t) = \sum_{i=1}^{N} \phi_i^*(\mathbf{r},t)\boldsymbol{\sigma}\phi_i(\mathbf{r},t), \tag{1}$$

where $\boldsymbol{\sigma}$ are the Pauli matrices and i is the joint index of $\mathbf{k}$ points and Kohn-Sham (KS) states. Within the full noncollinear spin configuration, the KS orbitals $\phi(\mathbf{r},t)$ are treated as two-component Pauli spinors propagated using the following equation:

$$i\frac{\partial\phi_j(\mathbf{r},t)}{\partial t} = \left\{\frac{1}{2}\left[-i\nabla + \frac{1}{c}\mathbf{A}_{\text{ext}}(t)\right]^2 + v_{\text{s}}(\mathbf{r},t) + \frac{1}{2c}\boldsymbol{\sigma}\cdot\mathbf{B}_{\text{s}}(\mathbf{r},t)\right\}\phi_j(\mathbf{r},t), \tag{2}$$

where $\mathbf{A}_{\text{ext}}(t)$ is the vector potential representing the external laser pulse and $v_{\text{s}}(\mathbf{r},t) = v_{\text{ext}}(\mathbf{r},t) + v_{\text{H}}(\mathbf{r},t) + v_{\text{xc}}(\mathbf{r},t)$ is the effective KS potential consisting of the external potential v_{ext}, Hartree potential v_{H}, and the exchange-correlation (XC) potential v_{xc}. Additionally, the KS magnetic field is $\mathbf{B}_{\text{s}}(\mathbf{r},t) = \mathbf{B}_{\text{ext}}(t) + \mathbf{B}_{\text{xc}}(\mathbf{r},t)$, the sum of the external magnetic field plus laser magnetic field $\mathbf{B}_{\text{ext}}$ and the XC magnetic field $\mathbf{B}_{\text{xc}}$.

To study magnons in real-time using TDDFT, we developed the method described in [19] in which supercells commensurate with the wave vectors $\mathbf{q}$ of particular magnon modes are constructed. In this work, we extend the method to include laser pulses, which can excite the electrons to a nonequilibrium state, allowing us to deduce the effect of this on the magnon modes.

The magnon frequencies are obtained by Fourier transforming the transverse atomic moments following the laser pulse. The frequency of the unperturbed modes agrees with linear-response TDDFT calculations, thus validating the approach. While TDDFT is a formally exact state-of-the-art method for treating magnonics in out-of-equilibrium systems, the price to pay for such a treatment is that it is highly computationally demanding. This restricts the size of the supercell that is practical and hence limits our study to high-energy/high-$\mathbf{q}$ modes. However, the physics of the problem remains valid even at lower $\mathbf{q}$ values.

The four-atom supercell of $Fe_{50}Ni_{50}$ is formed by extending the $L1_0$ primitive cell along the c axis, where lattice parameters are $a = 3.85$ Å and $c = 7.71$ Å. The Brillouin zone was sampled on a $\mathbf{k}$-grid of $8 \times 8 \times 8$, and a time step of 1.209 as was used for time propagating the orbitals using the algorithm presented in Ref. [27]. The adiabatic local spin density approximation to the XC functional was used. All simulations were done using the all-electron ELK electronic structure code [28].

III. RESULTS AND DISCUSSION

To understand the effect on the $Fe_{50}Ni_{50}$ magnons of pumping the electrons to a nonequilibrium state using an ultrashort laser pulse, we must first study the unperturbed magnon modes. These are shown in Fig. 1 for a four-atom supercell of $Fe_{50}Ni_{50}$. The size of the supercell determines how many magnon modes are present in our calculations; however, it is also constrained by the computational power available. With a four-atom supercell, we sample the magnon wave vectors over the entire first Brillouin zone: the four modes correspond to wave vectors $\boldsymbol{\Gamma}$, $\pm 1/2\boldsymbol{\Gamma}\mathbf{X}$, and $\mathbf{X}$, where $\mathbf{X} = (0, 0, 2\pi/a)$ in Cartesian coordinates for the fcc primitive unit cell. This wave vector determines the phase difference between adjacent atomic sites, as can be seen in the real-time TDDFT data presented in Fig. 2.

By choosing an appropriate initial state, we can control which modes are present in our calculations. For the

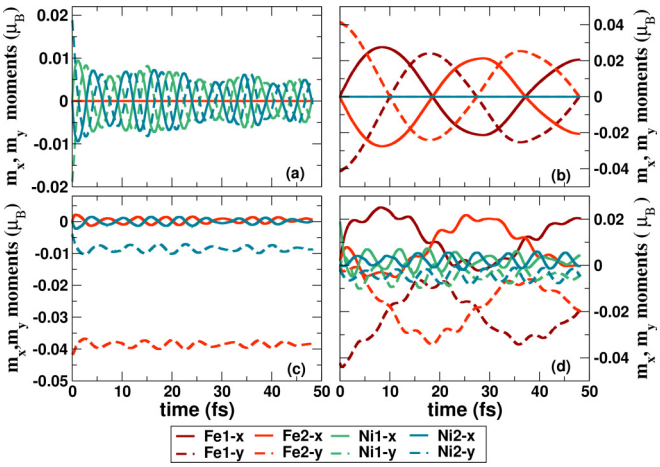

FIG. 2. Oscillation of the transverse (x, y) magnetic moments of the individual nickel and iron atoms in a four-atom supercell of $Fe_{50}Ni_{50}$ for different initial states. These magnons correspond to momenta $q = \Gamma$, $\pm 1/2\ \Gamma X$, and X. Decoupled, element-specific magnon modes can be seen for (a) nickel and (b) iron. Coupled Goldstone and optical modes can be seen in (c), and all four modes are excited in (d).

unperturbated system, this allows us to observe and isolate both coupled and decoupled modes (where only one of the magnetic sublattices oscillates): (1) The first is a high-energy pure Ni mode with $\omega = 710$ meV [Fig. 2(a)]. The energy of this mode is higher than the corresponding mode in bulk Ni (390 meV). (2) The second is a low-energy pure Fe mode with $\omega = 90$ meV [see Fig. 2(b)]; the frequency of this mode is also higher than the corresponding mode in bulk Fe (65 meV). The reason for the existence of these decoupled modes is the fact that at wave vector $\mathbf{q} = \pm 1/2\mathbf{\Gamma X}$, the effective exchange fields acting on an atom, from nearest-neighbor atoms of the other species, cancel, leading to only one of the magnetic sublattices oscillating.

The other two modes, out of the four allowed modes, are the coupled Fe and Ni modes: (3) the Goldstone mode ($\omega = 0$), in which all spins tilt together, as seen in Fig. 2(c) (dashed lines), and (4) the optical mode, where the Fe and Ni oscillate 180° out of phase with each other, as can also be seen in Fig. 2(c) (solid lines). The frequency of this mode is 760 meV, much higher than the $\mathbf{q} = \mathbf{X}$ mode in either Fe or Ni. All these modes can also be excited at the same time, as in Fig. 2(d).

In order to be able to manipulate magnons at ultrafast timescales we now investigate the behavior of magnon modes under short laser pulses. One of the fastest possible spin responses to lasers is via OISTR, primarily driven by minority-spin electrons optically excited from one magnetic sublattice to another, causing an increase in the moment on the first sublattice. In the present work the materials, as well as the laser pulses, are chosen to maximize OISTR: in the $Fe_{50}Ni_{50}$ alloy the magnetic moment on the Fe sublattice ($2.88\mu_B$) is much higher than on the Ni sublattice ($0.64\mu_B$). This causes laser-induced optical excitations to transfer minority-spin electrons from Ni to Fe, which in turn leads to an increase in the moment on the Ni site, with a corresponding decrease on the Fe site [see Fig. 3(b)]. The frequency of the laser pulse

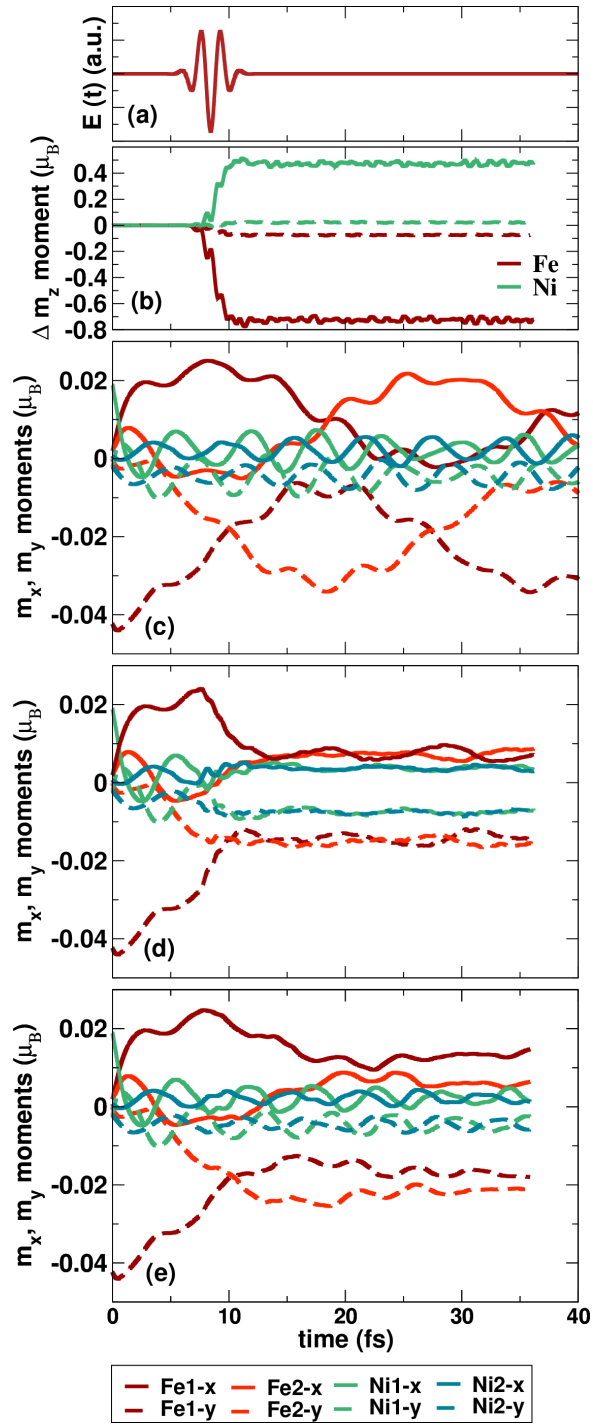

FIG. 3. (a) The electric field profile of the two laser pulses designed to induce OISTR transitions in $Fe_{50}Ni_{50}$; both have a frequency of 2.19 eV and FWHM of 2.41 fs but different fluences, 9.6807 and 0.9537 mJ/cm^2. (b) The change in the z magnetic moment for iron and nickel with the strong fluence pulse (solid lines) and weak laser pulse (dashed lines). (c) The unperturbed modes. The response of these modes to the (d) strong and (e) weaker laser pulses. In (d) only the Goldstone and optical modes survive, whereas in (e) the pure Fe mode is destroyed, while the pure Ni persists.

(2.19 eV) is tuned to optimize this charge transfer. Following laser excitation via this OISTR mechanism, the system will

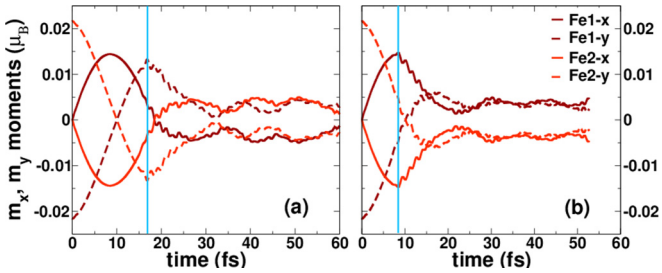

FIG. 4. The canting vector is dependent on the delay time of the laser and is shown relative to the pure Fe mode oscillations. A laser of fluence 0.9537 mJ/cm^2 is applied at (a) 16.8 fs and (b) 8.4 fs on the pure iron mode. The vertical lines represents the peak of the laser pulse.

relax back to the ground state on a picosecond timescale. From our calculations, we see three major effects on magnon dynamics due to OISTR excitations.

A. Element-selective optical destruction of magnons

The effect of OISTR on the various magnon modes can be seen in Fig. (3): a strong laser pulse (incident fluence of 9.6807 mJ/cm^2 and FWHM of 2.41 fs) effectively destroys both decoupled modes [see Fig. 3(d)]; the amplitude of the pure Fe magnon mode collapses with only small oscillations remaining which are also quickly damped. Looking at the Ni moments, which initially are a superposition of the pure Ni mode and the optical mode, we see that now only the optical mode exists as the two Ni atoms behave identically (recall that in the pure Ni mode, the two are 180° out of phase).

These magnon modes show a different dynamics when subjected to a weaker laser pulse of incident fluence, 0.9537 mJ/cm^2; the pure nickel mode now survives, while the Fe mode is still destroyed [see Fig. 3(e)]. In this case the Fe atoms cant with respect to each other with a new, but much reduced, pure Fe mode oscillating about this new configuration. By examining the number of spin-up/-down electrons excited on each atom, we find that the Fe atoms have significantly more local optical excitations than Ni. This causes the Fe-Fe exchange coupling to be modified more strongly than the Ni-Ni coupling, explaining the difference in behavior between the two modes. Thus, we have found a method by which we can selectively destroy either both Fe and Ni modes or just the Fe mode on a femtosecond timescale by tuning the fluence of the laser pulse. This is an important finding as it not only offers a mechanism of control over magnons but also highlights the fact that the dynamics of element-specific magnetization in alloys can greatly differ due to the choice of the pump pulse [23,25].

B. Modification of the canting vector

A change in the relative directions of the moments (i.e., the angle between the intersite spins in a multisublattice system) in a material can be obtained by rapid destruction of selected magnon modes. We demonstrate in Fig. 4 that the canting vector, $\mathbf{m}^{\mathrm{Fe1}}(t) - \mathbf{m}^{\mathrm{Fe2}}(t)$, can be controlled using the time delay of the laser pulse. The effect of the laser pulse is to destroy the magnon mode, but the phase of the magnon mode at the point when the laser is applied determines in which direction the Fe moments eventually point and thus determines the direction of the canting vector. In the first scenario the center of the pulse is chosen to be located at 16.8 fs when Fe1y and Fe2y are at their maximum amplitudes [see Fig. 4(a)], and in the second case the center of the pulse is chosen to be at 8.4 fs, which corresponds to the point in time when the Fe1x and Fe2x moments are at their maximum amplitudes [see Fig. 4(b)]. These two time delays in the laser pulses (with respect to the start of the simulation) result in different directions of the canting vector. For this canting behavior, the laser pulse used is weak, with fluence = 0.9537 mJ/cm^2, but the FWHM remains 2.41 fs, much shorter than the period of the pure Fe magnon mode, allowing this effect to be realized. Unlike in the strong laser case in Fig. 3(d), where the amplitude of the Fe mode is reduced to zero, in Fig. 4, the Fe moments remain finite but cease precessing, resulting in a final canted transient state. The main reason is that the laser excitation disrupts the exchange coupling between the nearest Fe atoms, causing the magnon mode to *freeze* into a spin spiral configuration. Extending the delay by half a period of the magnon oscillation will result in a canting vector pointing in the opposite direction. This indicates that with a careful choice of laser pulse a ferromagnetic metal can be made to be transiently noncollinear with a certain degree of control over the angle between intersite spins.

C. Ultrafast change in magnon frequency

The frequency of the magnon modes can also be manipulated by the pump-laser pulse. To demonstrate this we excite the optical mode and then look at its dynamics under the influence of pump pulses of differing fluences. The results for two different laser intensities (0.9537 and 9.68 mJ/cm2) are shown in Figs. 5(a) and 5(b), where it is clear that the oscillations are strongly influenced by the laser. Fourier transform of the transverse moment during these oscillations gives the frequency of the magnon mode, which is plotted as a function of laser intensity in Fig. 5(c). The main reason behind this change in frequency is the weakened exchange field between the magnetic sublattices [29–31] due to two processes, both of which lead to increased screening between the electrons of each atom: (1) excitation of electrons to excited delocalized states and (2) transfer of localized charge from one atom to the other.

This change in exchange coupling implies that the stronger this charge transfer is, the greater the change in the magnon frequency is, a fact that is reflected in the linear dependence of the magnon frequency on the pump-pulse fluence [Fig. 5(c)]. In this case OISTR is dominated by a double excitation where spin is excited from Fe to Ni and vice versa and hence quadratic in the electric field and thus linear in intensity/fluence. At some higher intensity where the charge excitation process saturates, the change in the magnon frequency also saturates. Thus, optical excitations offer a direct way to alter the frequency of a coupled magnon mode of two sublattices by tuning the fluence of the laser pulse. Since OISTR effects are very strong on antiferromagnetic (AFM) coupled systems, we expect very large changes in magnon modes when they are pumped with lasers. This mechanism

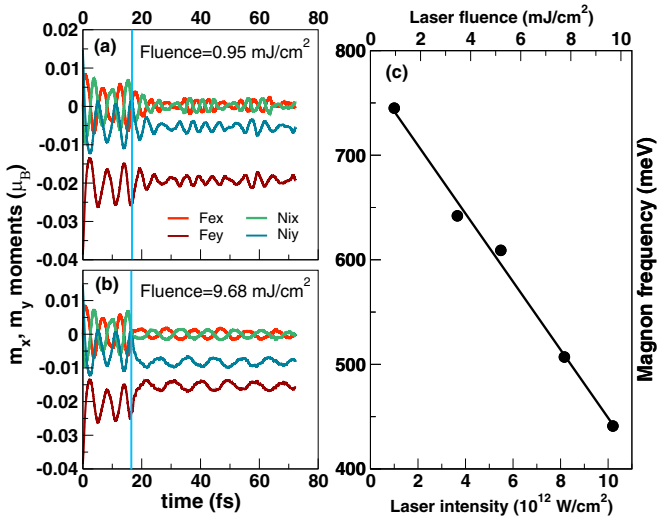

FIG. 5. The resulting change in the coupled Fe-Ni magnon frequency can be seen in the local moment dynamics following the applied laser pulse (the vertical line corresponds to the peak of the applied laser pulse) for two laser pulses with intensities of (a) 0.9537 mJ/cm^2 and (b) 9.680 mJ/cm^2. (c) Fourier transforming the dynamics following the laser pulse allows the altered magnon frequency to be extracted. These new frequencies are plotted against the laser intensity, for which a linear dependence was found.

for ultrafast modification of the magnon frequencies comes directly from the electronic excitation, in contrast to the indirect method, which uses the temperature dependence of the anisotropy field [32,33].

IV. CONCLUSION

To summarize, we have extended the domain of TDDFT simulations to include magnon dynamics in nonequilibrium systems. This opens the field of laser-coupled magnonics to *ab initio* theory. We first showed the prediction by TDDFT of element-specific magnon modes with vastly different energies in the $Fe_{50}Ni_{50}$ alloy. We then demonstrated three ways in which ultrafast laser pulses can manipulate magnon dynamics: (1) selective destruction of particular magnon modes where the Ni or Fe modes could be selectively destroyed depending on the laser intensity, (2) laser-driven destruction of the magnon mode leading to a transient noncollinear state of a ferromagnet, and (3) OISTR-driven renormalization of the optical magnon frequency, where we found a linear dependence between the laser intensity (or moment transferred) and the decrease of the magnon frequency.

Due to computational restrictions, relatively high wave vector modes were studied in this work. These modes are difficult to experimentally observe due to significant Landau damping due to interaction with the Stoner continuum. However, by elucidating the underlying physics in our examples, we are confident that the observed effects will be present throughout the Brillouin zone. In all cases the outcomes were achieved on ultrafast timescales, thus demonstrating the potential of laser control of magnonics for future technology. Antiferromagnetic spintronics/magnonics is an exciting and rapidly developing field [34–43]; thus, in future work, we plan to study the more exotic magnons in AFM systems and magnetic insulators (which are more long-lived due to the lack of Landau damping) and high wave vector modes excited via spin-transfer torque.

ACKNOWLEDGMENTS

N.S. acknowledges Grant No. DFG SFB762 for funding. S.S. acknowledges funding from Grant No. DFG TRR227 (Project No. A04). P.E. acknowledges funding from DFG Eigene Stelle Project No. 2059421. The authors acknowledge the North-German Supercomputing Alliance (HLRN) for providing High-performance Computing (HPC) resources that have contributed to the research results reported in this paper.

All calculations were performed by N.S. N.S. and P.E. wrote the paper with discussions and improvements from all authors.

[1] H. J. Qin, K. Zakeri, A. Ernst, L. M. Sandratskii, P. Buczek, A. Marmodoro, T. H. Chuang, Y. Zhang, and J. Kirschner, Nat. Commun. **6**, 6126 (2015).
[2] W. Heisenberg, Z. Phys. **49**, 619 (1928).
[3] R. Mondal, M. Berritta, and P. M. Oppeneer, Phys. Rev. B **94**, 144419 (2016).
[4] D. Hinzke, U. Atxitia, K. Carva, P. Nieves, O. Chubykalo-Fesenko, P. M. Oppeneer, and U. Nowak, Phys. Rev. B **92**, 054412 (2015).
[5] R. F. L. Evans, W. J. Fan, P. Chureemart, T. A. Ostler, M. O. A. Ellis, and R. W. Chantrell, J. Phys.: Condens. Matter **26**, 103202 (2014).
[6] E. Runge and E. K. U. Gross, Phys. Rev. Lett. **52**, 997 (1984).
[7] P. Elliott, F. Furche, and K. Burke, *Excited States from Time-Dependent Density Functional Theory*, Reviews in Computational Chemistry, Vol. 26 (Wiley, Hoboken, NJ, 2009).
[8] S. Sharma, J. K. Dewhurst, and E. K. U. Gross, Top. Curr. Chem. **347**, 235 (2014).
[9] P. Elliott, T. Müller, J. K. Dewhurst, S. Sharma, and E. K. U. Gross, Sci. Rep. **6**, 38911 (2016).
[10] J. K. Dewhurst, P. Elliott, S. Shallcross, E. K. U. Gross, and S. Sharma, Nano Lett. **18**, 1842 (2018).
[11] J. K. Dewhurst, S. Shallcross, E. K. U. Gross, and S. Sharma, Phys. Rev. Appl. **10**, 044065 (2018).
[12] D. Steil *et al.*, Phys. Rev. Research **2**, 023199 (2020).
[13] J. Chen, U. Bovensiepen, A. Eschenlohr, T. Müller, P. Elliott, E. K. U. Gross, J. K. Dewhurst, and S. Sharma, Phys. Rev. Lett. **122**, 067202 (2019).
[14] F. Siegrist, J. A. Gessner, M. Ossiander, C. Denker, Y.-P. Chang, M. C. Schröder, A. Guggenmos, Y. Cui, J. Walowski, U. Martens, J. K. Dewhurst, U. Kleineberg, M. Münzenberg, S. Sharma, and M. Schultze, Nature (London) **571**, 240 (2019).
[15] F. Willems, C. von Korff Schmising, C. Strüber, D. Schick, D. W. Engel, J. K. Dewhurst, P. Elliott, S. Sharma, and S. Eisebitt, Nat. Commun. **11**, 871 (2020).
[16] N. Singh, P. Elliott, T. Nautiyal, J. K. Dewhurst, and S. Sharma, Phys. Rev. B **99**, 035151 (2019).

[17] P. Buczek, A. Ernst, and L. M. Sandratskii, Phys. Rev. B **84**, 174418 (2011).
[18] S. Y. Savrasov, Phys. Rev. Lett. **81**, 2570 (1998).
[19] N. Singh, P. Elliott, J. K. Dewhurst, E. K. U. Gross, and S. Sharma, Phys. Status Solidi B **257**, 1900654 (2020).
[20] N. Tancogne-Dejean, F. G. Eich, and A. Rubio, J. Chem. Theory Comput. **16**, 1007 (2020).
[21] E. Beaurepaire, J.-C. Merle, A. Daunois, and J.-Y. Bigot, Phys. Rev. Lett. **76**, 4250 (1996).
[22] C. D. Stanciu, F. Hansteen, A. V. Kimel, A. Kirilyuk, A. Tsukamoto, A. Itoh, and T. Rasing, Phys. Rev. Lett. **99**, 047601 (2007).
[23] I. Radu, K. Vahaplar, C. Stamm, T. Kachel, N. Pontius, H. A. Dürr, T. A. Ostler, J. Barker, R. F. L. Evans, R. W. Chantrell, A. Tsukamoto, A. Itoh, A. Kirilyuk, T. Rasing, and A. V. Kimel, Nature **472**, 205 (2011).
[24] M. Hofherr, S. Häuser, J. K. Dewhurst, P. Tengdin, S. Sakshath, H. T. Nembach, S. T. Weber, J. M. Shaw, T. J. Silva, H. C. Kapteyn, M. Cinchetti, B. Rethfeld, M. M. Murnane, D. Steil, B. Stadtmüller, S. Sharma, M. Aeschlimann, and S. Mathias, Sci. Adv. **6**, eaay8717 (2020).
[25] S. Mathias, C. La-O-Vorakiat, P. Grychtol, P. Granitzka, E. Turgut, J. M. Shaw, R. Adam, H. T. Nembach, M. E. Siemens, S. Eich, C. M. Schneider, T. J. Silva, M. Aeschlimann, M. M. Murnane, and H. C. Kapteyn, Proc. Natl. Acad. Sci. U.S.A. **109**, 4792 (2012).
[26] I. Radu, C. Stamm, A. Eschenlohr, F. Radu, R. Abrudan, K. Vahaplar, T. Kachel, N. Pontius, R. Mitzner, K. Holldack, A. Föhlisch, T. A. Ostler, J. H. Mentink, R. F. L. Evans, R. W. Chantrell, A. Tsukamoto, A. Itoh, A. Kirilyuk, A. V. Kimel, and T. Rasing, SPIN **05**, 1550004 (2015).
[27] J. K. Dewhurst, K. Krieger, S. Sharma, and E. K. U. Gross, Comput. Phys. Commun. **209**, 92 (2016).
[28] ELK, version 6.0.17, elk.sourceforge.net.
[29] F. Dalla Longa, J. T. Kohlhepp, W. J. M. de Jonge, and B. Koopmans, Phys. Rev. B **81**, 094435 (2010).
[30] J. H. Mentink and M. Eckstein, Phys. Rev. Lett. **113**, 057201 (2014).
[31] N. Tancogne-Dejean, M. A. Sentef, and A. Rubio, Phys. Rev. Lett. **121**, 097402 (2018).
[32] M. van Kampen, C. Jozsa, J. T. Kohlhepp, P. LeClair, L. Lagae, W. J. M. de Jonge, and B. Koopmans, Phys. Rev. Lett. **88**, 227201 (2002).
[33] F. Hansteen, A. Kimel, A. Kirilyuk, and T. Rasing, Phys. Rev. B **73**, 014421 (2006).
[34] A. V. Kimel, A. Kirilyuk, A. Tsvetkov, R. V. Pisarev, and T. Rasing, Nature (London) **429**, 850 (2004).
[35] T. Kampfrath, A. Sell, G. Klatt, A. Pashkin, S. Mährlein, T. Dekorsy, M. Wolf, M. Fiebig, A. Leitenstorfer, and R. Huber, Nat. Photon. **5**, 31 (2011).
[36] T. Satoh, S.-J. Cho, R. Iida, T. Shimura, K. Kuroda, H. Ueda, Y. Ueda, B. A. Ivanov, F. Nori, and M. Fiebig, Phys. Rev. Lett. **105**, 077402 (2010).
[37] D. Bossini, S. Dal Conte, Y. Hashimoto, A. Secchi, R. V. Pisarev, T. Rasing, G. Cerullo, and A. V. Kimel, Nat. Commun. **7**, 10645 (2016).
[38] V. Baltz, A. Manchon, M. Tsoi, T. Moriyama, T. Ono, and Y. Tserkovnyak, Rev. Mod. Phys. **90**, 015005 (2018).
[39] R. A. Duine, K.-J. Lee, S. S. P. Parkin, and M. D. Stiles, Nat. Phys. **14**, 217 (2018).
[40] T. Jungwirth, J. Sinova, A. Manchon, X. Marti, J. Wunderlich, and C. Felser, Nat. Phys. **14**, 200 (2018).
[41] M. B. Jungfleisch, W. Zhang, and A. Hoffmann, Phys. Lett. A **382**, 865 (2018).
[42] R. Lebrun, A. Ross, S. A. Bender, A. Qaiumzadeh, L. Baldrati, J. Cramer, A. Brataas, R. A. Duine, and M. Kläui, Nature (London) **561**, 222 (2018).
[43] P. Němec, M. Fiebig, T. Kampfrath, and A. V. Kimel, Nat. Phys. **14**, 229 (2018).